Kinetics of Fast Short-Term Depression Are Matched to Spike Train Statistics to Reduce Noise

Reza Khanbabaie, William H. Nesse, Andre Longtin and Leonard Maler

J Neurophysiol 103:3337-3348, 2010. First published 31 March 2010;
doi: 10.1152/jn.00117.2010

J Neurophysiol 103: 3337–3348, 2010.
First published March 31, 2010; doi:10.1152/jn.00117.2010.

Kinetics of Fast Short-Term Depression Are Matched to Spike Train Statistics to Reduce Noise

Reza Khanbabaie,[1,2,3] William H. Nesse,[1,2] Andre Longtin,[1,2] and Leonard Maler[1]
[1]*Departments of Cellular and Molecular Medicine and* [2]*Physics, University of Ottawa, Ottawa, Ontario, Canada; and* [3]*Faculty of Science, Babol Noshirvani University of Technology, Babol, Mazandaran, Iran*

Submitted 27 January 2010; accepted in final form 29 March 2010

Khanbabaie R, Nesse WH, Longtin A, Maler L. Kinetics of fast short-term depression are matched to spike train statistics to reduce noise. *J Neurophysiol* 103: 3337–3348, 2010. First published March 31, 2010; doi:10.1152/jn.00117.2010. Short-term depression (STD) is observed at many synapses of the CNS and is important for diverse computations. We have discovered a form of fast STD (FSTD) in the synaptic responses of pyramidal cells evoked by stimulation of their electrosensory afferent fibers (P-units). The dynamics of the FSTD are matched to the mean and variance of natural P-unit discharge. FSTD exhibits switch-like behavior in that it is immediately activated with stimulus intervals near the mean interspike interval (ISI) of P-units (~5 ms) and recovers immediately after stimulation with the slightly longer intervals (>7.5 ms) that also occur during P-unit natural and evoked discharge patterns. Remarkably, the magnitude of evoked excitatory postsynaptic potentials appear to depend only on the duration of the previous ISI. Our theoretical analysis suggests that FSTD can serve as a mechanism for noise reduction. Because the kinetics of depression are as fast as the natural spike statistics, this role is distinct from previously ascribed functional roles of STD in gain modulation, synchrony detection or as a temporal filter.

INTRODUCTION

Short-term depression (STD) is observed at glutamatergic synapses ranging from brain stem (Hermann et al. 2007; Yang and Xu-Friedman 2008) to cortex (Abbott et al. 1997; Thomson and Deuchars 1997). STD is proposed to underlie diverse computations including removal of spike train correlations and transmission of novel signals (Abbott et al. 1997; Chung and Ferster 1998; Goldman et al. 2002; Tsodyks and Markram 1997). Here we report on a form of STD the time scale of which is faster than previously reported forms of short-term depression. The dynamics of this fast STD (FSTD) is matched to the presynaptic interspike interval (ISI) statistics.

We examine STD at synapses made by electroreceptors (P-units) onto pyramidal cells of the electrosensory lateral line lobe (ELL) of *Apteronotus leptorhynchus*. *Apteronotus* has a sinusoidal electric organ discharge (EOD) (Moortgat et al. 1998) that drives the baseline discharge (~200 Hz mean) of P-units (Gussin et al. 2007; Nelson et al. 1997). Prey and the EOD of conspecifics superimpose amplitude modulations (AMs) on the EOD (Benda et al. 2006; Nelson and MacIver 1999) that are encoded by the firing rate (low-frequency signals) and synchronization (high-frequency signals) of P-units (Benda et al. 2006; Gussin et al. 2007). The statistics of baseline and P-unit discharge evoked by naturalistic signals are well characterized (Benda et al. 2006; Gussin et al. 2007).

P-units project to three topographic maps within the ELL where they synapse directly on a subset of pyramidal cells (this subset is referred to as E-cells) and inhibitory interneurons (Bell and Maler 2005). The coding properties of pyramidal cells in the ELL maps are also well characterized (Krahe et al. 2008; Marsat et al. 2009). Computational studies have, however, revealed a discrepancy between P-unit activity and its behavioral decoding—the rate coding of low-frequency AMs by P-units is not sensitive enough to account for prey capture (Gussin et al. 2007; Ludtke and Nelson 2006; Maler 2009). On this basis, it has been suggested that synaptic mechanisms such as STD may be involved in enhancing weak signal detectability by P-units and their target cells (Ludtke and Nelson 2006).

P-unit synapses on E-cells are glutamatergic with AMPA and *N*-methyl-D-aspartate (NMDA) receptor mediated excitatory postsynaptic potentials (EPSPs) as well as disynaptic inhibition (Berman and Maler 1998a). We have been able to isolate and observe the dynamics of the AMPA receptor component of P-unit evoked EPSPs and found that they exhibit only STD. Unlike previously observed slower STD dynamics (Abbott et al. 1997; Hermann et al. 2007; Yang and Xu-Friedman 2008), the onset and recovery of P-unit depression occurs on a timescale similar to their mean interspike interval (~5 ms). By using stimulation frequencies that straddled the natural P-unit discharge rate (Gussin et al. 2007), we found that this dramatic behavior was mediated by a novel STD with both ultra-fast onset and offset kinetics. We propose that the FSTD dynamics can aid in the detection of weak prey signals as previously suggested on theoretical grounds (Ludtke and Nelson 2006). A computational analysis reveals a possible functional role of FSTD to reduce variability in the synaptic output rate. This allows for increased sensitivity to weak input changes that could aid in the detection of prey signals. Previously reported functional roles of STD in gain modulation, synchrony detection, or as a temporal filter (Abbott and Regehr 2004; Abbott et al. 1997; Carlson 2009; Fortune and Rose 2000; Rose and Fortune 1999; Senn et al. 1998) require the time scale of STD to be slower than the time scale of the ISI statistics. In contrast, our newly proposed functional role of noise reduction relies on the ISI statistics matching the kinetics of FSTD. We rigorously define our use of term "matching" at the end of RESULTS. Thus our newly proposed functional mechanism of noise reduction is distinct from these previously reported functional roles.

Address for reprint requests and other correspondence: R. Khanbabaie or W. H. Nesse, Dept of Cellular and Molecular Medicine, University of Ottawa, 451 Smyth Rd., Ottawa, Ontario K1H 8M5, Canada (E-mail: skhanbab@uottawa.ca or wnesse@uottawa.ca).

METHODS

ELL slice preparation

The gymnotiform fish, *A. leptorhynchus* (male or female, 10–15 cm in length) were anesthetized in oxygenated water containing 0.2% 3-aminobenzoic ethyl ester (Tricaine Methanesufonate, MS-222; Sigma). Surgical procedures and slice preparation were performed as previously described (Berman and Maler 1998c, 1998b; Berman et al. 1997). Briefly, the ELL was removed, and slices of 300–340 μm in its transverse plane were prepared on a vibratome (modified to provide high-amplitude blade vibrations, Technical Products International, St. Louis, MO) while immersed in ice cold artificial cerebrospinal fluid (ACSF; containing, in mM: 124 NaCl, 3 KCl, 0.75 KH_2PO_4, 2 $CaCl_2$, 1.5 $MgSO_4$, 24 $NaHCO_3$, and 10 D-glucose) containing 1 mM kynurenic acid. Slices were maintained in an interface chamber in ACSF without kynurenic acid at room temperature for 30 min to an hour before recording. All experimental protocols were approved by the University of Ottawa Animal Care Committee.

Stimulation, recording, and data analysis

Electrical stimulation of the primary afferents of the ELL was achieved by placing a gold tipped bipolar lacquer-coated sharpened tungsten electrode (50 μm exposed tips) into the deep fiber layer (containing electroreceptor afferents) of the ELL, lateral to the recording site in the pyramidal cell layer (PCL) and at a sufficient distance to avoid direct stimulation of the impaled neuron (see Fig. 1). Square wave pulses (20 μs, 1–80 V cathodal, model DS2, Digitimer, Welwyn Garden City, UK) were delivered via the stimulating electrode. Stimulus intensity was adjusted to evoke ~70% of maximal response amplitude of the evoked EPSP so that the short latency of EPSPs (~1.5 ms from the onset of stimulus) does not cause uncertainty about its starting point. Because excessively high stimulation parameters caused direct activation of the cells (spike with a latency of <0.9 ms), we first adjusted the stimulus intensity so that it was far below this level but still sufficient to evoke a clear EPSP. For most of cells, we have used low stimulation intensity (20–40 V). For four cells, we had to use higher stimulation intensity (40–75 V). The stimulus artifact was routinely monitored to be certain that our results were not due to systematic changes in stimulus intensity. The gold plating of the stimulus electrodes was sufficient to maintain a constant artifact as assessed by visual inspection of the voltage traces. We directly measured the artifact in 10 randomly picked pulse trains and measured the height of the 20th artifact of these trials and normalized the height difference of the first and the 20th stimulus artifact to the first artifact height accordingly. The average relative artifact difference was ~0.026 ± 0.01 (SD) mV. The change in the stimulus intensity in pulse trains was <3% of the initial stimulus intensity.

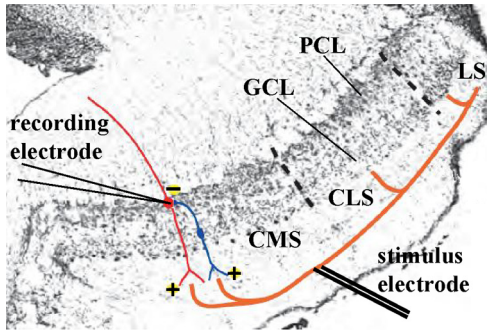

FIG. 1. Transverse Cresyl violet stained section through the electrosensory lateral line lobe (ELL) to illustrate the experimental setup. P-unit afferents (orange) topographically innervate the centromedial segment (CMS), centrolateral segment and lateral segment maps and make excitatory (glutamatergic) synapses onto the basal dendrites of pyramidal cells (red) and GABAergic interneurons (blue). The interneurons then make inhibitory synapses ($GABA_A$) onto the somata of the pyramidal cells. Here we stimulate a small bundle of P-units (black arrow) and record from pyramidal cells in CMS. PCL, pyramidal cell layer; GCL, granule cell layer.

Intracellular recordings were made using sharp microelectrodes (80–150 MΩ) filled with 3 M CsAcetate (CsAc) with tips placed in the PCL of the ELL centromedial segment (CMS). Most of recordings were made with QX314 (100 mM in 3 M CsAc, Alomone Labs, Jerusalem, Israel), tetraethylammonium (TEA, 50 μM, Sigma-Aldrich, St. Louis, MO) and picrotoxin (PTX, 100 μM, Sigma-Aldrich) in the pipette to block active conductances (Berman et al. 2001) as well as $GABA_A$ receptor mediated disynaptic inhibitory PSPs (IPSPs) (Berman and Maler 1998b). Pyramidal cells stopped spiking in ~2–5 min after penetration. Intracellular picrotoxin eliminated the disynaptic IPSP in ~6–9 min as previously reported in other preparations (Akaike et al. 1985; Cupello et al. 1991; Inomata et al. 1988; Khanbabaie et al. 2007). Some recordings were made with picrotoxin (1 mM, dissolved in ACSF), 2-amino-5-phosphonovaleric acid (APV; 100 μM, Tocris, Bristol, UK) and cyclothiazide (50 μM, Tocris) in the bath to confirm the effectiveness of intracellular picrotoxin in blocking the IPSP. We did not use bath applied picrotoxin or $GABA_A$ receptor antagonists to block inhibition because application of these drugs to the ELL cell layers results in epileptiform discharge of pyramidal cells (unpublished observation). Additional experiments were done with or without cyclothiazide to investigate the potential role of AMPA receptor desensitization at P-unit synapses onto pyramidal cells.

The P-units are phase locked to the EOD and so occur at multiples of the constant EOD interval, and so we usually stimulated at multiples of a fixed interval. We chose 1.5 ms as the basic interval, representing an EOD frequency of 667 Hz which is at the low end for this species (~600–1,000 Hz). This interval was chosen so that we could still see an EPSP (uncontaminated with the stimulus artifact) with stimulation at two EOD intervals (3 ms). The stimuli were created as output sequences in Spike2 using both text files and graphical sequence editor. Because we found that it takes ≤30 s for full recovery of EPSPs after each trial, we waited 40 s between each trial. Our stimulus protocols were designed to answer our specific questions as follows: *1*) paired pulse protocol with stimulation intervals ranging from 3 to 30 ms to quantify paired pulse depression; *2*) repetitive fixed stimulation intervals (3–30 ms) to investigate the onset and recovery kinetics of depression; *3*) stimulating with a fixed number of pulses (20 pulses) at shorter intervals (3–7 ms) till steady state and then stimulating at longer intervals (100 ms) for 2 s to investigate the long-time scale recovery from depression; *4*) stimulating with a variable number of high-frequency conditioning pulses (2–20 pulses) followed by lower-frequency pulses to test history-dependent effects; and *5*) stimulation with one-second-long epochs of Poisson sequences with a mean interval of 5 ms (i.e., the mean P-unit interspike interval).

All experiments were software controlled (Power 1401, CED, UK) running Spike 2 on an IBM microcomputer. Electrical activity was amplified (Axoclamp 900A, Molecular Devices), filtered (10 kHz cutoff), digitized (20 kHz) and analyzed off-line (Spike 2, Cambridge Electronic Design, and Igor Pro 6.0.3.1, WaveMetrics). Each EPSP was measured as the voltage difference between the baseline, measured 0.3 ms before the stimulus artifact, and the peak voltage of the EPSP. Further analysis, curve fitting, and visualization was performed using IgorPro software. All mathematical modeling and theoretical calculations were performed using Matlab programming software (MathWorks). The synthetic P-unit ISI distribution (light blue, Fig. 7*B*) was computed from Monte Carlo simulations of a P-unit spiking model adapted from Chacron et al. (2001).

RESULTS

Electrophysiology

We recorded from 43 E cells within the pyramidal cell layer of the centromedial segment of the ELL (Fig. 1). P-unit in vivo baseline discharge rates follow a lognormal distribution with a mean of 200 Hz (5 ms ISI) with most rates ranging between 100 and 300 Hz or 3.3 to 10 ms ISIs (Gussin et al. 2007). Stimulating P-units fibers in vitro with frequencies at their mean baseline discharge rate (200 Hz) evokes, as previously reported (Berman and Maler 1998a), a complex sequence of EPSPs of varying amplitudes and spikes (Fig. 2*A*) as well as IPSPs (Fig. 2*B*). Because we were interested in the dynamics of short-term plasticity at P-unit synapses, we used intracellular blockers of active conductances (CsAc, QX314, and TEA) to block spikes and associated after-potentials as previously described (Berman et al. 2001). In addition we used intracellular application of picrotoxin to block the stimulus evoked disynaptic $GABA_A$ IPSP (Berman and Maler 1998a). Intracellular picrotoxin appeared to completely eliminate the IPSP as expected from other preparations (Akaike et al. 1985; Khanbabaie et al. 2007), but to confirm its effectiveness, we added picrotoxin to the bath ($n = 5$); this treatment had no further effect on the evoked EPSP (Fig. 2*B*). The amplitude of the evoked EPSPs still varied appreciably even after these treatments with successive individual EPSPs appearing to decrease in amplitude but riding on a slower depolarization (Fig. 2*C*, $n = 11$). We suspected from earlier work (Berman and Maler 1998a) that the slower summating component of the evoked compound EPSP represented the NMDA receptor component of the P-unit evoked response. Adding APV to the bath to block the NMDA receptor component of the evoked EPSP (Berman and Maler 1998a; Berman et al. 2001) eliminated the slow depolarization as might therefore be expected. Under APV block the evoked EPSPs revealed simple depression (for stimulus intervals <30 ms), that reached a steady-state amplitude after 10–20 stimulus pulses (Fig. 2*D*). Under these conditions, the E cell acts as a simple indicator of mainly presynaptic dynamics (except for desensitization of AMPA receptors, see following text) and the intracellular/extracellular drug combination was therefore always utilized in subsequent experiments.

Characterizing synaptic depression: paired pulse and steady-state experiments

P-units discharge in phase with the EOD (~600-1,000 Hz species range). For our initial protocols, we assumed an EOD of 666 Hz and therefore stimulated at intervals equal to multiples of 1.5 ms. P-unit evoked EPSPs have a very short latency (Berman and Maler 1998a) (~1–2 ms), and the minimum inter-stimulus interval was 3 ms (2 EOD intervals); this is typical of most P-units and also prevents contamination by the stimulus artifact. Stimulation at ≤20 EOD intervals (30 ms) were used to span the natural range of baseline and evoked P-unit discharge (Gussin et al. 2007).

Depression induced by a single stimulus and its recovery was investigated using a standard paired pulse depression (PPD) protocol with intervals ranging from 3 to 30 ms. We normalized with respect to the initial value of evoked EPSP to permit averaging over different pyramidal cells ($n = 9$). Standard models of STD assume that each action potential causes the depletion of some presynaptic resource D (e.g., vesicles, Ca^{2+} channels). On spiking, the resource D decrements by a constant multiplicative factor $(1 - p)$: $D \rightarrow (1 - p)D$, where p is the fraction of resource decremented. The resource consumed, pD, is proportional to the EPSP amplitude: $A \propto pD$. After the spike, and possibly a brief refractory time, there is an exponential recovery of the resource with time scale τ until the next spike (Abbott et al. 1997; Tsodyks and Markram 1997).

We fitted an exponential curve to the normalized EPSP of the paired pulse depression (PPD) versus interval duration. As shown in Fig. 3*A*, the data can be well fit by the exponential curve of the standard model: $A = B - (1 - p)\exp[-(\Delta t - 3)/\tau]$, where B is the value of the EPSP amplitude at the longest interval used in these experiments (30 ms) and Δt is the interstimulus pulse interval. A refractory time of 3 ms was chosen because this is the minimal time at which we can stimulate and therefore estimate depression; the physiological

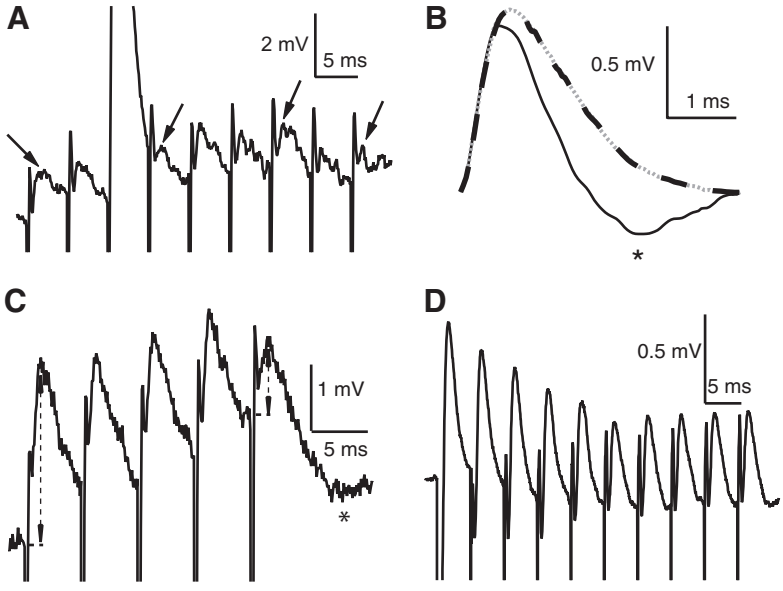

FIG. 2. Depression of the pyramidal cell excitatory postsynaptic potentials (EPSPs) evoked by stimulation of P-unit afferents at their mean frequency. *A*: characteristic response of a pyramidal cell—mixed EPSPs, inhibitory PSPs (IPSPs; occluded, see *B*) and spikes—on stimulation of a small bundle of P-units with a pulse train of 5 ms intervals. The stimulus artifact and spike are truncated. Note the irregular variation in the peak amplitude of the evoked EPSP (arrows point to 1st, 4th, 7th and last EPSP peaks). *B*: each synaptic response includes a very fast EPSP (AMPA- black solid) followed by a fast IPSP ($GABA_A$) (asterisk) as previously described (Berman and Maler 1998a). Adding picrotoxin to the pipette solution removed the inhibitory part of response (dotted light gray). Adding picrotoxin to the bath subsequently had no further effect (dashed dark gray). *C*: EPSPs in the presence of intracellular blockade of voltage-gated ion channels (see METHODS) as well as picrotoxin. Spikes are eliminated and the stimulus train-evoked EPSPs appear more regular. Note that the amplitude of 1st EPSP is bigger than the 5th EPSP (dashed arrows to baseline membrane potential) although this change is masked by a slow long-lasting depolarization (*). *D*: 2-amino-5-phosphonovaleric acid (APV) blocks the slow P-unit evoked depolarization revealing nonsummating AMPA receptor mediated (Berman and Maler 1998a) EPSPs. The amplitude of evoked EPSPs is steadily depressed during the stimulus train and reaches a steady state after 10- 15 pulses.

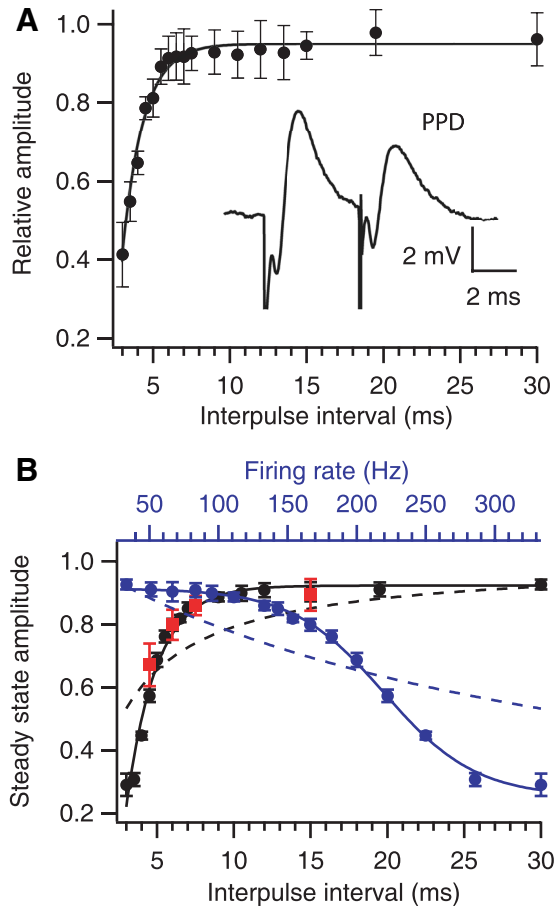

FIG. 3. Paired-pulse and steady-state depression. *A*: normalized amplitude of EPSPs vs. stimulus pulse intervals. We plot, for every stimulation interval, the ratio of the 2nd EPSP to the 1st evoked EPSP (thus normalized to the 1st EPSP) and average the ratios over $n = 9$ cells; error bars are SD. Note strong depression for the shortest interval (3 ms) and nearly complete recovery of EPSP amplitude (>0.9 of initial value) with interpulse intervals >10 ms. *Inset*: An example of typical paired pulse depression. *B*: the normalized steady-state amplitude of EPSPs after 15 pulses at intervals from 3 to 30 ms (bottom axis, filled black circles) or rates from 33 to 333 Hz (top axis, filled blue circles). Black circles are the mean of the last 5 (of 20) normalized EPSPs (ratio to the 1st evoked EPSP) as a function of stimulus interval. Blue circles are the same data re-plotted as a function of stimulus frequency (top axis). Error bars are, in both cases, SD. The solid curves (black and blue) are exponential and sigmoidal fit on the data in time and frequency domain, respectively. The dashed curves are the best possible resource depletion model fits on the data. Note that the inflection point of the sigmoid fit in the frequency domain is close to the mean P-unit discharge rate (200 Hz). The number of cells recorded in this case varied with the stimulus interval as follows: $n = 8$ (3 ms), 5 (3.5 ms), 6 (4 ms), 28 (4.5 ms), 9 (5 ms), 7 (5.5 ms), 19 (6 ms), 6 (6.5 ms), 6 (7 ms), 16 (7.5 ms), 18 (9 ms), 11 (10.5 ms), 15 (12 ms), 24 (15 ms), 10 (19.5 ms), 12 (30 ms). The red squares are the normalized amplitudes of the 1st EPSPs of the 2nd pulse train (see Fig. 4*B*, $n = 6$) after a reversed protocol where longer intervals (1st pulse train) were given first (till steady state) followed by shorter intervals (2nd pulse train). Note that the reversed protocol EPSPs fall on the same exponential curve as those from the short to long interval protocol.

refractory time would be one EOD cycle (1.5 ms in this case). The choice of this recovery time is important only for the curve fitting and does not change any of our data analysis or modeling results. Note that recovery is still not complete at the longest stimulus interval (30 ms) because the fit gives $B = 0.94 \pm 0.01$ (see following text for the kinetics of long-term recovery from depression). The best fit was achieved with $P = 0.45 \pm 0.02$ and the time constant of fast recovery from depression was $\tau = 1.35 \pm 0.10$ ms. This is an order of magnitude faster than previously reported values for depression due to vesicle depletion and/or receptor desensitization (Abbott et al. 1997; Wang and Manis 2008; Yang and Xu-Friedman 2008); in these papers, the fastest estimated time constants of depression range from $\tau = 10$ ms, through 25 ms, and up to ~300 ms. Recovery is also faster than previously reported values for depression associated with putative vesicle release refractory processes: $\tau =$ 5 to 20 ms (Dobrunz et al. 1997; Hjelmstad et al. 1997).

This fast recovery time scale of $\tau = 1.35$ ms is seemingly at odds with the deep levels of steady-state depression induced by repetitive trains of pulses. We stimulated with 20 pulses over a wide range of frequencies and used the mean normalized amplitude of the last five EPSPs as an estimate of the steady-state response. The experimental steady-state amplitude (Fig. 3*B*) follows a similar exponential curve to that of the PPD (Fig. 3*A*, black dots). Moreover, the same data are plotted in frequency space (Fig. 3*B*, blue dots, top axis), showing a sigmoid-like drop in steady-state amplitude with an inflection point of 220 Hz (the solid blue line is the sigmoidal fit), near the 200 Hz mean rate of P-units, suggesting that the depression kinetics are tuned to the mean value of the input spike train frequency. We used the estimated value $\tau = 1.35$ ms to compute the predicted steady-state EPSP amplitude D_∞ of the resource-depletion model (Abbott et al. 1997; Tsodyks and Markram 1997) as a function of the stimulation interval Δt and the depletion parameter p

$$D_\infty = (1 - e^{-\Delta t/\tau})/[1 - (1 - p)e^{-\Delta t/\tau}] \quad (1)$$

The highest stimulation frequencies induced depression far in excess of that predicted by the resource depletion model even with the best fit achievable by varying the p parameter ($P = 0.002 \pm 0.0003$), while low-frequency stimulation induced far less depression than predicted by the model (black dashed line in Fig. 3*B*). When viewed in frequency space, the model fails to capture the sigmoidal shape of the experimental data because the resource-depletion model exhibits a $1/f$ input rate-amplitude relationship (Abbott et al. 1997; Matveev and Wang 2000; Tsodyks and Markram 1997) (blue dashed line in Fig. 3*B*). Also fitting the data over both p and τ does not improve the fit appreciably (data not shown). Furthermore, the estimated P value is highly different from that estimated in the PPD experiments (0.002 vs. 0.45). The resource-depletion model fails to capture these STD dynamics because it assumes that p is constant for all input frequencies. We suggest that the large drop in steady-state EPSP amplitude for high-input frequencies is not accounted for by an exponentially recovering resource model alone. Furthermore, because the drop in amplitude that occurred for two pulses (i.e., PPD) is greater than expected by the fixed-p model, we infer the kinetics of the variable P value are very fast. Because we infer the dynamics of depression are fast, on the time scale less than any experimentally given interpulse interval, we can further infer that the depression time course cannot be accounted for with a modified resource depletion model that includes additional multiple-timescale dynamics involving calcium-mediated slow-time scale activity-dependent processes (Dittman and Regehr 1998; Yang and Xu-Friedman 2008).

Induction and recovery from depression

The induction of depression and recovery from depression both exhibit very fast kinetics. Because the inflection point of the STD recovery curve is near the mean P-unit ISI interval of 5 ms (Fig. 3*A*), the STD might rapidly modulate EPSP amplitudes under natural conditions. Stimulation at 4.5 ms intervals (3 EOD cycles, ~220 Hz) induced strong depression but a single longer interval (9 ms or 6 EOD cycles) was sufficient for nearly full recovery (~0.9, Fig. 4*A*, $n = 11$). Stimulation at 6 and 7.5 ms intervals (4 and 5 EOD cycles) induced far weaker STD that also rapidly recovered, while stimulation at 15 ms (10 EOD cycles) induced minimal depression. To test for possible hysteresis of the STD dynamics, we then reversed the stimulation protocol giving long followed by short stimulus intervals. This induced an apparent mirror image effect with stimulus intervals ≥9 ms producing minimal depression (~0.9 – 0.95) followed by strong STD only for the 9–4.5 ms stimulus trains (Fig. 4*B*, $n = 6$).

Notice that the onset of depression in all these experiments includes an exponential-like decline in synaptic strength, but the 9 to 4.5 ms transition (pulse 21 in total or 1st pulse of 2nd train, Fig. 4*B*) reveals that the bulk of the depression arises as a sudden drop in synaptic strength. As we shall show, the exponential decline accounts for ~10% of the depression and is an artifact of the unnatural quiescent period prior to the experimental stimulation. This sudden drop in the 9-4.5 ms transition is uncovered because the exponential transient has mostly decayed during the preceding 20 pulses at 9 ms intervals. This large frequency-dependent drop is associated with the novel fast STD that we are most interested in, and is the component that the resource-depletion model fails to capture. Plotting the relative EPSP amplitude of the 21st pulse (the transition point) versus the stimulation interval (Fig. 3*B*, red squares) reveals that within one pulse interval at a faster rate (4.5 ms), the amplitude achieves near the same depression level as that of the steady state after 20 pulses because both lie on the same exponential curve.

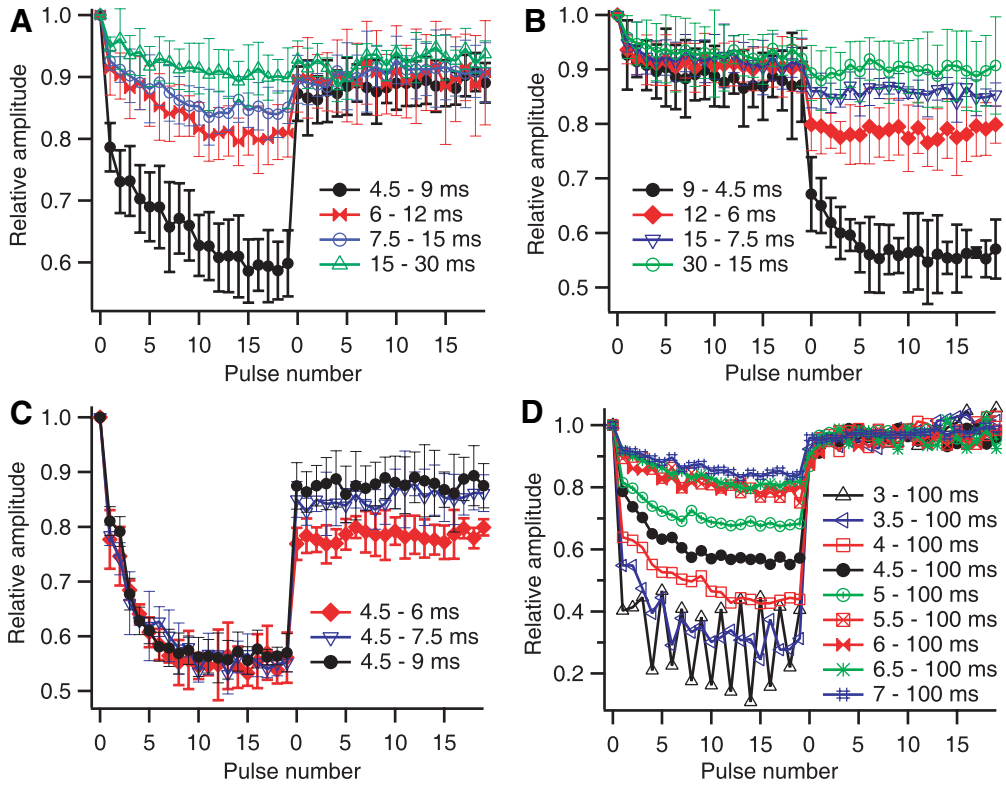

FIG. 4. Switch-like behavior and fast recovery from depression. *A*: normalized amplitude of EPSPs vs. pulse number. Normalized amplitude (with SD error bars) is plotted as in Fig. 3 and $n = 11$. The stimulus was 2 sets of pulse trains. A short interval pulse train that reached a steady-state level of depression (20 pulses) followed by a pulse train with intervals at twice the duration (short-long intervals) pulse train (20 pulses). Note the dramatic increase in steady-state depression as the stimulus interval decreases from 6 to 4.5 ms. In contrast, there are only smaller gradual changes in depression when going from 6 to 12 ms stimulus intervals. Note that recovery from depression with 4.5 ms stimulus intervals takes only a single 9 ms interval and that recovery is to approximately the same level for the 4.5 to 9, 6 to 12, and 7.5 to 15 ms short-long protocols. Also note that there is still a small amount of depression at the termination of the stimulation protocols. *B*: same protocol as *A* with reverse stimulation protocol (long-short intervals) to check for possible hysteresis of the depression dynamics ($n = 6$). These recordings were done in different pyramidal cells from those in *A*. Note symmetry of the depression kinetics. *C*: same protocol as *A* with fixed stimulus interval (4.5 ms) followed by different longer intervals (fixed-variable intervals) to better estimate the stimulus interval duration required for recovery after steady-state depression has been reached ($n = 7$). Note that some recovery can occur after an interval equal to 1 extra electric organ discharge (EOD) cycle (4.5–6 ms) and that recovery is nearly identical for slightly longer stimulus intervals of 7.5 and 9 ms. *D*: same protocol as *A* with different stimulation intervals followed by very long fixed interval of 100 ms (variable-fixed intervals) ($n = 6$). A set of short intervals (3–7 ms with 0.5 ms increment—these could not occur when the P-units are driven by a natural, constant EOD) was used to test depression at a higher temporal resolution followed by the same long (100 ms) interval to test for long-term recovery from depression. Note that there is a near linear decrease in steady-state depression as the stimulus interval goes from 3 to 6 ms, but that subsequent increases in stimulus interval produce only minor changes in depression. Also note the ringing EPSP response at the 3 ms stimulus interval. This effect only occurred for these shortest stimulus intervals and did not always occur; we have no explanation for this result. Note that steady-state recovery is identical after all initial short stimulus intervals and full recovery is only approached after 20 stimulus pulses or 2 s.

The kinetics of recovery from depression were also very fast. We measured the recovery from STD by switching from the steady-state response induced from 20 pulses at 4.5 ms to 6, 7.5, and 9 ms. There was already rapid recovery from STD for a single 6 ms interval, and this was complete with a single 7.5 ms interval (Fig. 4*C*, $n = 7$). Further, there were no obvious memory effects in that the depression at a particular stimulus interval is the same no matter what the prior stimulation history (compare Fig. 4, *A–C*). Thus both the induction and recovery from depression occur on time scales equal or less than the natural input interval timescale, meaning that changing input intervals are immediately tracked by the depression kinetics, for both increasing and decreasing intervals.

The induced STD is a highly nonlinear function of input frequency. To demonstrate this, we abandoned the use of natural stimulation intervals to investigate STD at higher temporal resolution (Fig. 4*D*, $n = 6$). These experiments revealed that strong STD is only induced over a very narrow range of stimulus intervals (~3-7 ms or ~333-140 Hz), while lower frequencies (33–140 Hz) induce minimal STD that is nearly independent of stimulus frequency. Within this narrow range (3–7 ms), there is a nearly perfect linear increase of STD with decreasing stimulus interval (Fig. 4*D*). Most remarkably this switching occurs between 4.5 and 6 ms or a single EOD cycle. This implies that with natural variation around the baseline P-unit discharge of ~200 Hz (Gussin et al. 2007), most P-units will straddle this nonlinear zone and rapidly switch between strong (0.3–0.55) and weak (~0.9) states of depression due to natural P-unit firing variability. It therefore appears that FSTD kinetics might be matched to the variance of P-unit discharge as well as to its mean. Low-frequency sensory input will reduce the P-unit firing rate sufficiently (Gussin et al. 2007) to allow for near full recovery (~0.90) of synaptic potency. These effects appear to occur in a memory-less fashion so that synaptic efficacy can track P-unit firing rate without distortion by slow STD dynamics.

While a bulk of the observed depression has fast kinetics, ~10% of the depression appeared to recover at a much longer time scale. This is already suggested by the slow onset STD kinetics during low-frequency stimulation. Stimulation at 15 ms (Fig. 4*A*, green triangles) produced a slow onset weak depression (~0.9) that we attribute primarily to resource depletion. Stimulation at 4.5 ms intervals produced an initial rapid depression that we attribute to fast STD, followed by a slower component that we attribute to a resource depletion effect (Fig. 4*A*, black circles). We directly investigated the longer-term recovery by using 100 ms stimulus intervals after steady-state STD had been reached. Again there was no indication of memory effects because the recovery curves were nearly identical no matter what the prior state of depression (Fig. 4*D*). Full recovery was very slow with a mean time constant of 380.07 ± 61.7 ms. This value is comparable to that reported for other depressing synapses (Abbott et al. 1997; Yang and Xu-Friedman 2008) and has been attributed to the replenishment of vesicle stores (Dittman and Regehr 1998; Yang and Xu-Friedman 2008) or removal of Ca^{2+} channel inactivation (Xu and Wu 2005). P-units have a high baseline firing rate, maintaining firing rates >20 Hz even with strong natural sensory input (Gussin et al. 2007). The large tau for slow recovery therefore implies that P-unit synapses always operate in a depressed state and that depression to ~0.9 of absolute maximum is effectively their maximum strength under natural conditions.

Several recent studies have demonstrated that recovery from vesicle depletion is enhanced during high-frequency stimulation, perhaps due to Ca^{2+}-dependent presynaptic processes (Dittman and Regehr 1998; Stevens and Wesseling 1998; Yang and Xu-Friedman 2008). We tested whether the FSTD might exhibit such dependence by stimulating 2–20 times at 4.5 ms intervals followed by a recovery stimulus interval of 9 ms. As seen in Fig. 5, recovery is nearly identical for all stimulus numbers ($n = 7$) and recovery is always to ~0.9 no matter the prior state of depression. There is therefore no evidence of activity-dependent recovery for the FSTD, again reinforcing the idea that it does not depend on vesicle depletion and recovery.

Contributions of desensitization to STD

Desensitization of AMPA receptors also contributes to STD although the reported magnitude of this effect is variable (Isaacson and Walmsley 1996; Oleskevich et al. 2000; Yang and Xu-Friedman 2008). We therefore used cyclothiazide (CTZ) to investigate the possible contribution of desensitization to FSTD. Although CTZ is known to have other actions, its main effect is believed to be the prevention of AMPA receptor desensitization (Yang and Xu-Friedman 2008). CTZ slightly reduced depression (Fig. 6, *A* and *B*); for example, for 4.5 ms stimulus intervals, the normalized mean steady-state EPSP amplitude was slightly but significantly increased from 0.57 ± 0.01 to 0.62 ± 0.03 in the presence of CTZ ($n = 12$, $P < 0.02$; *t*-test) with a similar differential for the 9 ms recovery stimulation. The switch-like behavior and rapid recovery from depression were all preserved in the presence of CTZ (Fig. 6, *A* and *B*). We were not able to study the recovery from desensitization in isolation from the FSTD. However, because the CTZ and no-CTZ curves are parallel during the entire 9 ms stimulus period (Fig. 6*A*), we can conclude that desensitization must recover with a time constant >9 ms. The

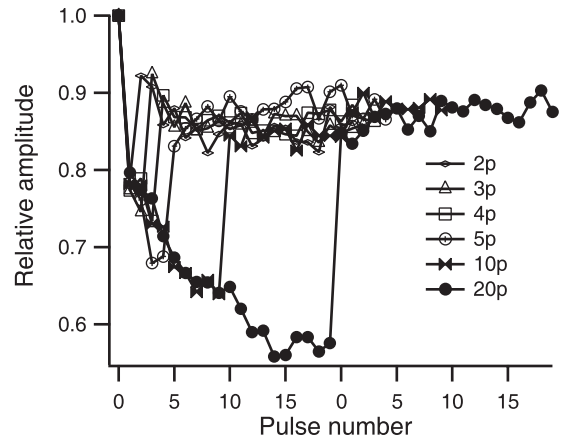

FIG. 5. This experiment was designed to probe whether recovery from depression was dependent on the amount of prior activity. The graph shows normalized amplitude of EPSPs vs. pulse number with the stimuli containing 2 sets of pulse train ($n = 5$). The 1st pulse train contains different number of pulses (2–20 pulses) with a fixed interval of 4.5 ms. The 2nd pulse train contains a fixed number of pulses (20 pulses) with a fixed interval of 9 ms. The number of initial stimulation pulses has no effect on the rate of recovery from depression or the steady-state recovery level after 3–5 stimulus pulses.

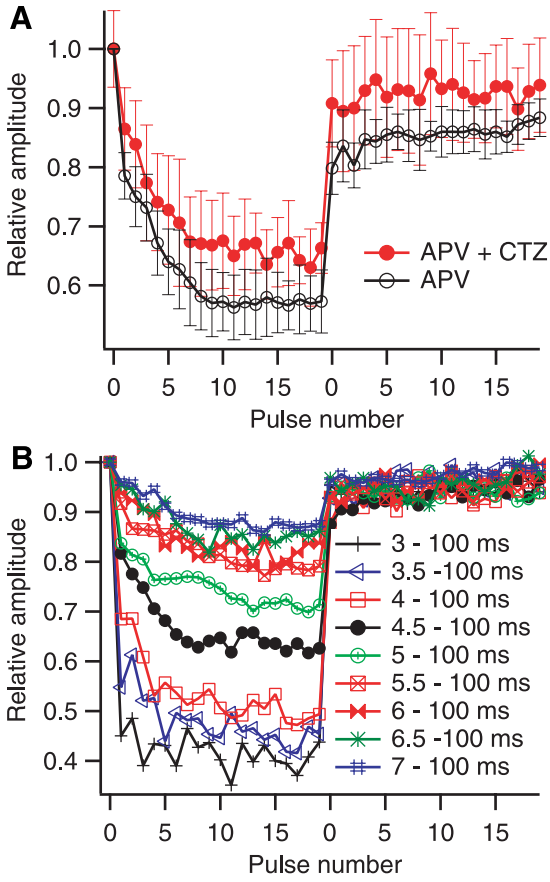

FIG. 6. Switch-like dynamics and fast recovery after blocking desensitization of AMPA receptors. *A*: cyclothiazide (CTZ) reduces depression suggesting that desensitization of AMPA-Rs contributes to depression at P-unit synapses onto pyramidal cells (n = 12). However, CTZ reduces steady-state depression by approximately the same amount for the 4.5 ms stimulus pulse intervals (1st 20 stimuli) as for the 9 ms intervals (2nd 20 stimuli). The switch like behavior is thus preserved and desensitization does not play a major role in depression dynamics at these synapses. *B*: same as Fig. 4*D* but in the presence of CTZ. Blocking AMPA-R desensitization slightly reduces the depression for all short intervals (3–7 ms) but does not have any effect for long stimulus intervals (100 ms).

slow recovery process, including the first stimulus at 100 ms postdepression, was completely unaffected by application of CTZ (Fig. 6*B*); this demonstrates that the desensitization recovery time constant is $\ll$100 ms. These results are consistent with studies in the auditory system where time constants for recovery from desensitization are on the order of 10 ms and do not contribute greatly to the control of EPSP amplitude at high stimulation frequencies (Yang and Xu-Friedman 2008).

We conclude that although desensitization of AMPA receptors contributes to STD at P-units synapses, its effect is small and additive to the larger fast depression; most importantly, desensitization does not alter the dynamics of FSTD at P-unit synapses.

Random stimulation protocol

The results reported in the preceding text suggest that there is a nonlinear relationship between the stimulus interval and the magnitude of the succeeding EPSP. To test this idea more rigorously, we used Poisson stimulation for 1-s epochs with a mean firing rate of 200 Hz and intervals <3 ms omitted (n = 4). We used Poisson rather than natural P-unit stimulus because Poisson stimulation produces a finer temporal resolution than the discretized P-unit stimulation protocol, and we wanted to examine FSTD dynamics in a generic context. At the start of the 1-s stimulation epoch the EPSP amplitudes quickly decreased in size in an exponential-like fashion, similar to the decay observed at the beginning of the regular pulse trains. Figure 7*A* shows the input timings (abscissa) versus EPSP amplitude (ordinate) for a random pulse train for one exemplar cell. The initial transient decay is presumably an artifact of the long silent rest period that is not present for normal P-unit discharge. After the first five random pulses, the EPSP amplitudes reach a variable but much lower amplitude.

Figure 7*B* shows the EPSP amplitudes from the stimulation train minus the first 10 pulses, associated with the large transient. The EPSP amplitudes (ordinate) were averaged over five trials of one cell, the same exemplar cell as in Fig. 7*A*, as a function of the interpulse interval (Δt, abscissa); the responses of all four cells were entirely similar. We have normalized the amplitude with respect to the exponential fit of the data (red) so that the exponential fit asymptotes to unity. The amplitude-interpulse interval relationship appears to be matched to the ISI statistics of P-units. The ISI statistics of an example model P-unit firing at 200 Hz detailed in Fig. 7*B*, with the ISI probability density function (PDF; light blue) along with the associated cumulative distribution function (CDF; dark blue). Notice that the exponential fit of the amplitude data matches with the general trend of the CDF. Note, however, that individual P-units fire at a range of intrinsic rates around 200 Hz, so the specific shape of individual CDFs will vary. Still, the qualitative timescale matching in Fig. 7*B* is apparent. We have recorded from five other cells (data not shown), at a range of Poisson input frequencies (166–220 Hz) and with natural P-unit ISI trains (144–200 Hz). In each case, the amplitude-IPI relationship had a similar relation with exponential time constant fits in the range 1–2.3 ms, all centered near the mean P-unit firing frequency (4.5–5 ms) and encompassing most of the natural P-units baseline firing range; this again suggests a qualitative match of fast STD dynamics and P-unit spike train statistics (mean, variance, and possibly higher moments). As stated in the preceding text, the resource-depletion model failed to capture the repetitive pulse data because the p factor was assumed constant. A more detailed analysis of the response of pyramidal cells to natural P-unit stimulation and a matching wider frequency range of Poisson input will be presented elsewhere.

To model the random stimulation data, we abandoned the exponential recovery dynamics of the resource-depletion model in favor of a variable probability p of release model. Based on our results in the preceding text, after the initial transient depletion, the EPSP amplitudes appear to depend exclusively on the previous ISI. Here we test this theory by fitting the EPSP amplitude A_i of the ith pulse from the Poisson stimulation by a simple functional relationship

$$A_i \propto p(\Delta t_i) \quad (2)$$

where $p(\Delta t_i)$ can be viewed as the proportion of transmitter stores released on spiking. We will test two functional forms for $p(\Delta t)$. The first is a simple exponential model shown in Fig. 7*B* (red line)

$$A_i \propto H(\Delta t - \Delta t_0)(1 - e^{-\frac{\Delta t - \Delta t_0}{\tau}}) = p(\Delta t) \quad (3)$$

where H is the Heaviside step function. This functional form is also identical to data fits we have performed in Figs. 3, *A* and *B*, and 4. We also employ a piecewise linear model (Fig. 7*B*, green line) to the EPSP amplitude data

$$p(\Delta t) = m(\Delta t - b)H(\Delta t - b)H(1 - m(\Delta t - b)) + H(-1 + m(\Delta t - b)) \quad (4)$$

where m is the estimated slope of the linear zone, b is the estimated x intercept. This latter functional form produces the same qualitative results, but the linear approximation enables us to perform a more transparent mathematical analysis. Notice that the amplitude-IPI relationship is similar to both the PPD data and the steady-state amplitude data (see Figs. 3, *A* and *B*, and 4). Remarkably, it appears that the amplitude of each EPSP depends on the previous IPI interval according to either the exponential or the piecewise-linear model and not a function of any discharge pattern prior to that. To test that previous history does not influence the EPSP amplitude, we examined the variance accounted for by a linear model $A_i = k_0 + k_1\Delta t_i + k_2\Delta t_{i-1}$, for $i = 1 \ldots N$ in the stimulus epoch. The r^2 statistic with $k_2 = 0$ (i.e., a single-variable linear relationship) accounted for 61.92% of the variance, while optimal two-variable regression fits $k_2 \neq 0$ accounted for only 0.59% more variance and are not statistically significant (1-way model utility ANOVA: $F = 2.97$, $P > 0.05$). Furthermore, no discernible nonlinear relationship was evident on visual inspection of the amplitude versus two previous interpulse intervals in the $\Delta t_{i=1}$ dimension beyond the piecewise-linear relationship in the Δt dimension shown in Fig. 7*B*.

The instantaneous relationship between EPSP amplitude and the single previous interpulse interval (Fig. 7*B*) has important consequences for stimulus coding. Interestingly, the depression assigns a weight to each synaptic input, encoding the temporal interval that precedes it. Furthermore, the depression curve (red or green line, Fig. 7*B*) appears to be matched to the normal P-unit spike statistics (P-unit CDF, dark blue line). Using our linear model, note that most interspike intervals of P-units (light blue line in Fig. 7*B*) lie within the linear zone. One consequence of this functional weighting is noise-reduction of P-unit synaptic output. Theoretical studies suggest that *Apteronotus* can detect weak prey signals transmitted by P-units over short time windows of ~200 ms (Nelson and MacIver 1999). Within this time window, a typical prey signal may only produce a one or two extra spikes within a single P-unit noisy spike train of near 40 spikes (mean rate: 200 Hz) (Ludtke and Nelson 2006; Nelson and MacIver 1999). Here we show that FSTD observed in P-units can reduce noise of the synaptic output independent of the specific input spike. Let $q(\Delta t)$ be the distribution of ISIs. For our Poisson stimulation example $q(\Delta t) =$

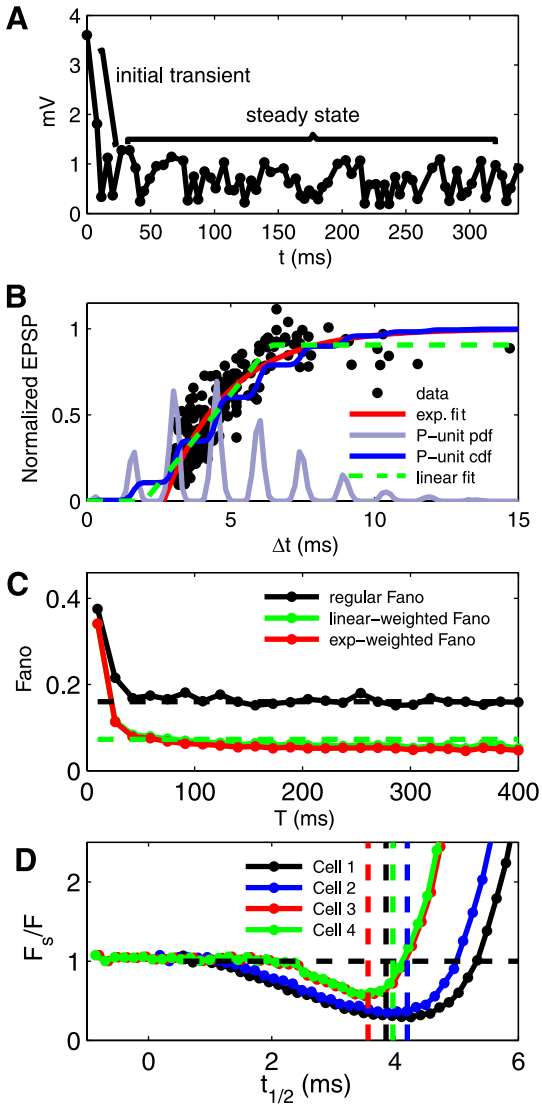

FIG. 7. Random stimulation and modeling. *A*: stimulation with pulses derived from a truncated Poisson process (mean frequency: 200 Hz with intervals <3 ms removed). The EPSP amplitudes vs. stimulus pulse timings for 1 exemplar cell. The initial transient decay happens during 1st 5–10 pulses (arrow) and is followed by EPSPs with amplitudes that vary in an irregular manner. *B*: the EPSP amplitudes from the random (truncated Poisson intervals) stimulation (black filled circles) vs. input interpulse interval of 1 exemplar cell (*cell 2* of *D*). The 1st 10 pulses were omitted to ignore the large initial transient decay. The red curve is an exponential fit and the green curve is the piecewise linear model fit to the data. EPSP amplitudes were normalized to the exponential fit so that the fit asymptotes to unity. Note that the midpoint of these curves are near 5 ms—the mean interspike interval of P-unit baseline discharge. Most baseline interspike intervals of P-units (light blue line- this is the simulated baseline ISI of a model 200 Hz P-unit) lie within the linear zone of the linear model. The cumulative distribution function of the P-unit ISI (dark blue curve) reveals that the time scale of depression curve (red or green) is matched to the input statistics. *C*: regular and the synaptic-weighted Fano factor. The black filled circles show the regular Fano factor (uniformly weighted) and the black dashed line represents the asymptotic limit for large detection windows. A true Poisson process has a constant Fano factor of 1; the reduction seen here is due to the truncation of stimulus intervals <3 ms. The synaptic-weighted Fano factor along with its asymptotic limit are shown in red and green for the exponential and piecewise linear depression models, respectively, along with the analytically derived theoretical asymptote (green dashed line). *D*: the ratio of the synaptic Fano over the regular Fano (ordinate, computed at $T = 200$ ms to ensure that the asymptote is reached) computed from the 200 Hz Poission random stimuli as a function of a temporal translation of the piecewise linear synaptic depression curve (absisca) $p(\Delta t;t_{1/2})$, where $t_{1/2}$ is the translation by the position of the half-maximum point of the curve. The experimentally estimated default half-maximum values for 4 cells (see legend) are indicated by the vertical dashed lines intersecting the abscissa. For all 4 cells the default values induce a variance reduction with the reduction very near the global minimum for most cells studied. Deviations from the default values lead to divergence of the synaptic Fano, suggesting that the default values are matched to the input spike rate to reduce variance.

$H(\Delta t - 3)\lambda e^{-\lambda\Delta t}$, where $\lambda = (f - 3)10^{-3}$ ms $^{-1}$ guarantees that the average firing rate is $f = 200$ Hz,but these results are generic to any renewal process $q(\Delta t)$. Without depression, we measure the mean synaptic input of a P-unit in a detection window T to be

$$X(T) = n(T)/T \tag{5}$$

where $n(T)$ is the random spike count in the time window the properties of which depend on the spike statistics $q(\Delta t)$. The spike count $n(T)$ is a commonly used proxy for the synaptic input to pyramidal cells in cortex (Shadlen and Newsome 1998). For the same time window with depression, each synaptic input amplitude in the window is weighted according to the model $A_i \propto p(\Delta t_i)$. Hence, the synaptic-weighted output rate is

$$Y(T) = \frac{1}{\bar{p}T}\sum_{i=1}^{n(T)} A_i \tag{6}$$

To make X and Y comparable, we specify that the long-time average output is the same. To do so, we have normalized Y by the factor $\bar{p}^{-1}$, where the average weighting $\bar{p} = \int_0^\infty p(t)q(t)dt$: for large T, the averages of X and Y are $\langle X\rangle = \langle Y\rangle = \langle n\rangle/T$. With identical averages, we show that the variances $\mathrm{Var}(X) > \mathrm{Var}(Y)$ for large enough detection windows. Without depression

$$\mathrm{Var}(X) = \frac{\mathrm{Var}(n)}{\langle n\rangle T}\frac{\langle n\rangle}{T} \approx \frac{f}{T}F(T) \tag{7}$$

where $f = \langle n\rangle/T$ is the average firing rate and $F(T) = \mathrm{Var}(n)/\langle n\rangle$ is the instantaneous rate of growth of the variance of the spike count, called the Fano factor, or the "index of dispersion" of the spike count (Gabbiani and Koch 1998). For uncorrelated spike trains, $F(T)$ converges to the coefficient of variation of the ISI squared, CV^2, of the spike train for large T. The CV is a nondimensional measure of spike variability defined as SD of the ISI over the mean ISI and can be obtained from moments of $q(\Delta t)$ (Gabbiani and Koch 1998). For the depression-weighted spike train, the output rate variance is

$$\mathrm{Var}(Y) = \mathrm{Var}\left(\frac{1}{T\bar{p}}\sum_{i=1}^{n(T)} A_i\right) \approx \frac{f}{T}F_s(T) \tag{8}$$

where $F_s(T)$ is the synaptically weighted Fano factor that measures the dispersion in the synaptic-weighted sum rather than the raw spike count. As noted in the preceding text, P-unit spiking is tuned to the fast STD in that most of the ISIs for the Poisson process, or the natural P-unit spike trains, fall within the linear zone of the piecewise-linear function of the depression model. By ignoring the small fraction outside the linear zone, we calculate the variance

$$\mathrm{Var}(Y) = \mathrm{Var}\left(\frac{\sum_{i=1}^{n(T)} m(\Delta t_i - b)}{m(\langle\Delta t\rangle - b)T}\right) = \left(\frac{\sum_{i=1}^{n(T)}\Delta t_i - bn(T)}{(\langle\Delta t\rangle - b)T}\right) \tag{9}$$

Because $\Sigma(\Delta t)/T \approx 1$ and $\bar{p} = m(\langle\Delta t\rangle - b)$, then

$$\mathrm{Var}(Y) \approx \frac{f}{T}F_s(T) = \frac{f}{T}\left(\frac{b}{\langle\Delta t\rangle - b}\right)^2 F(T) \tag{10}$$

This noise-reduction can be achieved for any renewal spike process $q(\Delta t)$ the spike intervals of which fall in the linear zone of the depression curve. For the particular parameters for depression revealed in our experiments, the factor $[b/(\langle\Delta t\rangle - b)]^2 \sim [2/(5 - 2)]^2 = 4/9 < 1$, thus lowering the variance by a factor of about 1/3. Figure 7*C* shows the regular Fano factor (black dots) and both the analytically derived linear-synaptic-weighted Fano factor (green dots), and the very similar numerically computed exponentially fit model (red dots) along with the asymptotic limits CV^2 for large detection windows (black and green dashed lines, respectively) (see Gabbiani and Koch 1998). The regular Fano factor can be understood as a uniformly-weighted version of the synaptic-weighted Fano. It is interesting to note that the synaptic weighted Fanos converge to ~1/3 of the regular Fano factor when the time window nears 200 ms, the critical time window for *Apteronotus* prey detection (Nelson and MacIver 1999). Note that the variance reduction property is mediated by the requirement that a majority of the possible ISIs fall in the linear zone of the depression curve (Fig. 7*B*, green line). For the choice of a 3-ms-delayed exponential input distribution used in our experiments, ~80% of the ISIs fall in this zone. By excluding 20%, we introduce a small systematic bias in the estimate of the synaptic-weighted Fano $F_s(T)$ by both ignoring the longer ISIs in the normalization factor $\bar{p}$ and in calculating the variance. This makes our estimation of the synaptic Fano asymptote (Fig. 7*C*, green flat line) only approximate. Note also that P-units can fire with periods of <3 ms as illustrated by an example ISI distribution in Fig. 7*B* (light blue), which is the stimulation limit imposed by experimental constraints. It is unknown what weighting or synaptic dynamics occurs for these fast intervals.

The variance reduction property predicted analytically in the preceding text depends on the mean input rate relative to the intrinsic tuning of the depression curve $p(\Delta t)$. The matching of the input rate to the depression tuning $p(\Delta t)$ is illustrated by computing the synaptic Fano factor over a range of translated depression curves $p(\Delta t; t_{1/2})$, where $t_{1/2}$ is the half-maximum inter-pulse interval value of the depression curve $\{p(t_{1/2};t_{1/2}) = \frac{1}{2}\max_{\Delta t}[p(\Delta t)]\}$. Figure 7*D* shows the values of the half-maximum points as vertical dashed lines intersecting the abscissa from estimated piecewise-linear depression curves of four distinct cells, each given the 200 Hz truncated Poisson inputs like that shown in Fig. 7*B* (*cell 2* is shown in *B;* 2 other cells were also given realistic P-unit input spike trains that produced the same qualitative results, but the analyses for natural P-unit stimulation protocols will be presented elsewhere). We then estimated the asymptotic synaptic-weighted Fano factor F_s, normalized to the regular Fano F, from Monte Carlo simulations ($T = 200$ ms windows) over a range of translated half-maximum points. The computed synaptic Fano factors exhibit a characteristic drop in variability near the estimated half-maximum values for all cells studied. Variance reduction will only occur when the linear zone of the depression curve is tuned near but below the mean input rate of the cell (200 Hz or 5 ms inter-pulse intervals in this case). For larger half-maximum values above the mean interpulse intervals, the synaptic Fano exhibits increased variance relative to the regular Fano. In this case, the depression reduces the EPSP amplitude severely for a majority of the likely interpulse intervals, effectively stopping synaptic transmission. This causes the normalization parameter $\bar{p}$ to go to zero, thereby causing the relative synaptic Fano to diverge to infinity as the half-maximum value increases. Conversely, decreasing the half-maximum point lower than the data-estimated values

eventually leads to the synaptic-weighted Fanos converging to the regular Fano. This is because half-maximal values well below the mean IPI leads to an effective uniform weighting of all likely IPIs, which is equivalently the regular Fano factor.

The range of half-maximum values that exhibit variance reduction (Fig. 7*D*) depends on the steepness of the linear zone of the depression curve. For *cells 1* and *2,* the estimated slopes were lower: $m = 0.194, 0.229$, respectively, relative to *cells 3* and *4* ($m = 0.418, 0.438$, respectively) and so the linear zones of *cells 1* and *2* comprised a broader range of input intervals, and in turn, a broader range mean input intervals can still induce a variance reduction. Thus although there is heterogeneity in the experimentally estimated depression curve steepness and half-maximum values, variance reduction is a general property for the synaptic depression observed in P-unit afferents, occurring whenever the depression curve $p(\Delta t)$ is tuned near the mean input frequency.

We can now specify precisely what we mean when we state (INTRODUCTION and RESULTS) that the proposed noise reduction property of FSTD at P-unit synapses results from a matching of P-unit baseline firing ISI statistics to the FSTD kinetics. We define noise reduction as a reduction in the variance of the synaptically weighted baseline P-unit spike count over some time window. We have shown that noise reduction will occur when the mean P-unit ISI is matched to the half-maximum depression versus interpulse interval curve (for that P-unit), and the ISI range for noise reduction will depend on the slope of the depression curve. Figure 7*D* demonstrates that such matching does in fact occur and that FSTD dynamics therefore effectively reduces noise (variability) of the incoming P-unit spike trains.

The depression curves we have reported were generated by stimulating many P-units ($\leq$25) (Maler 2009) with a mean interpulse interval of 5 ms; the recipient pyramidal cell thus effectively averages the evoked responses across all of its P-unit inputs. A critical question that arises is whether the FSTD kinetics (half-maximum depression value and slope of the depression curve) are matched to the mean and variance of ISI distribution of individual P-units, or alternatively, matched to the aggregate statistics of the entire input population of P-units. This question is, however, not technically accessible at present.

Although the variance of the EPSPs is reduced by the FSTD as shown in the preceding text, the EPSP amplitude is also reduced and therefore the gain, given by the factor $b/(\langle\Delta t\rangle - b)$, is also reduced in response to sensory signals. There is a striking similarity between this result and our previous demonstration of noise shaping by P-unit spike trains (Chacron et al. 2005). Although P-units have low gain for low-frequency signals, the negative correlations of their ISIs reduces their low power noise resulting in a great improvement in their signal to noise ratio for low-frequency input. The combined effect of this noise reduction with the FSTD gain and noise reduction on transmission of weak signals will be an important focus of future studies.

The switch-like behavior associated with FSTD (Figs. 4 and 5) can now be readily understood from the relationship between the discrete P-unit ISI distribution and the continuous piecewise linear EPSP amplitude versus previous ISI duration relation (Fig. 7*B* red curve vs. light blue ISI distribution). Most ISIs (2nd to 4th peak of light blue curve) fall in the first linear zone of the curve and are therefore depressed. Whenever a longer ISI occurs (5th or 6th peaks) it lands on the flat part of the red curve so that no depression is induced and the EPSP amplitude appears to discontinuously switch to a discrete higher value.

DISCUSSION

We have discovered a form of fast STD at electroreceptor synapses onto pyramidal cells. Two remarkable features of this FSTD are, first, that it appears to be matched to the natural spike train statistics (mean and variance) of P-units where "matching" is as defined in the preceding text in the computational section of RESULTS: baseline P-unit discharge statistics have average ISIs of 5 ms (Gussin et al. 2007) and most ISIs fall within the range of stimulation intervals ($\sim$3–8 ms) that induce FSTD; as already noted, some ISIs will be greater than those inducing FSTD, and this might result in rapid switching between EPSP amplitudes in vivo (see Figs. 3–5). As noted in the preceding text, we do not know whether the "matching" is at the level of the mean ISI averaged over many P-units or is specific for each P-unit. The second feature is that the EPSP amplitudes are a piecewise linear function to the duration of the previous ISI with a strong linear dependence within the $\sim$3–8 ms zone, thus rapidly and monotonically codifying temporal information into EPSP amplitudes.

The fast depression stands in contrast with the additional smaller and much slower component of STD at these synapses. This component recovers with a time constant of 380 ms, more typical of other synapses, i.e., 200–600 ms for cortex (Abbott et al. 1997), and spanning 100 s of P-unit ISIs. Presumably this STD component is mediated by the depletion of some resource such as vesicles and recovers via their replenishment (Tsodyks and Markram 1997). However, this form of depression is unlikely to be of significance for sensory coding by P-units because its magnitude will remain relatively constant at their high firing rates. In addition we describe a small component of the fast depression due to desensitization of AMPA receptors. Desensitization merely enhances depression at all stimulation frequencies but does not alter its dynamics in response to rapid changes of the input ISI sequence.

We have not established the biophysical basis for FSTD. Recovery from STD at synapses in brain stem auditory nuclei can often be well modeled as an exponential process with two or more time constants. The fastest reported process has a time constant of 10–15 ms (Cook et al. 2003; Yang and Xu-Friedman 2008) and has been attributed to desensitization of AMPA receptors (Yang and Xu-Friedman 2008); this interpretation is consistent with our results. Estimated time constants of slow recovery from STD range from 200 ms to $>$1 s (Abbott et al. 1997; Cook et al. 2003; Yang and Xu-Friedman 2008) and have usually been attributed to replenishment of vesicle stores (Zucker and Regehr 2002) or removal of inactivation of the Ca^{2+} channels essential for vesicle fusion (Forsythe et al. 1998). These processes are too slow to account for the fast onset and recovery of FSTD at P-unit synapses. The minimal depression due to the process with slow recovery (depression to $\sim$0.9 of the 1st evoked EPSP) does suggest an interesting possibility—that the FSTD is due to the reduction of the probability of vesicle fusion after a short stimulation interval, followed by a very rapid recovery of release probability (Hjelmstad et al. 1997). In this scenario, there are few vesicles available for release following a short stimulus interval, thereby minimizing vesicle depletion (Matveev and Wang 2000). Consistent with this interpretation, earlier work by Stevens and

colleagues (Dobrunz et al. 1997Stevens and Wang 1995) and Hjelmstad et al. (1997) has described hippocampal PPD as consisting of a brief refractory period (5–20 ms) during which no recovery could occur, followed by rapid recovery (time constant of 3.4 ms). It has been further suggested that this effect is not due to vesicle depletion but rather to a direct action of high levels of Ca^{2+} on the exocytotic machinery (Hsu et al. 1996) or vesicle release refractory processes (Dobrunz et al. 1997). A theoretical study (Matveev and Wang 2000) also indicates that resource depletion is not capable of accounting for fast depression at cortical synapses and proposed that this is due to an activity-dependent inactivation of the exoctyosis machinery. We propose that the inactivation of the exocytotic machinery accounts for the FSTD we have observed, as previously suggested for synaptic transmission in hippocampus (Dobrunz et al. 1997); furthermore, we also propose that the kinetics (refractory period and recovery time) of FSTD are tuned to the varying requirements of information transfer at specific synapses.

It is possible that the experiments required to reveal FSTD have not been performed in other systems. STD has been best characterized in slice preparations of the calyx of Held synapses in the medial nucleus of the trapezoid body (MNTB) (Yang and Xu-Friedman 2008). There is a tonotopic representation in the MNTB and, at least for low-frequency sounds ($<$1,000 Hz), the calyceal afferent discharge is phase locked to the acoustic input (Paolini et al. 2001) and will therefore skip at different ISIs. Stimulation of the calyceal afferents in vitro cannot mimic the in vivo discharge rate and pattern and may therefore have missed the stimulation frequency at which ultra-fast STD occurs. For example, if we had confined our stimulation frequency to $\leq$100 Hz, we would not have found this new form of STD; in the case of P-units our stimulation protocols were designed around their known in vivo mean discharge rate.

The functional consequences of FSTD are manifold. The standard function of slowly recovering STD detailed in previous studies is to filter out slow stimulus modulations while generating a phasic response to fast stimulus fluctuations (Abbott and Regehr 2004). Here the rate of recovery from STD set the timescale for the synaptic filtering: stimulus fluctuations slower than the rate of replenishment are canceled out, whereas fast changes are transmitted. At a population level, this leads to normalization across inputs and better sensitivity in the postsynaptic neuron to quick changes in firing rates of any of its inputs (Abbott et al. 1997). These standard functional roles ascribed to STD rest on the assumption that the spike interval time scale is shorter than the synaptic resource replenishment timescale τ. This is true for standard forms of STD; however, this is *not* the case for what we have observed at P-unit synapses. The kinetics of P-unit FSTD act on a time scale of 1.5 ms, which is the typical timescale of EOD discharge, the highest time scale resolution for the fish's electrosensory system. In contrast, P-units discharge around 5 ms intervals. Hence for the *Apteronotus*, FSTD does not compute phasic stimulus filtering as described in other systems (Abbott and Regehr 2004).

Instead we propose that the novel FSTD can serve to reduce noise in the synaptic output. A longer (shorter) ISI results instantaneously in a larger (smaller) EPSP amplitude by a linear one-to-one relationship, thereby reducing variability of the average synaptic output per unit time. This works independently but in combination previous investigations of noise-reduction attributed to ISI correlations observed in P-units (Chacron et al. 2001, 2004; Ratnam and Nelson 2000) or due to greater firing regularity of one class of vestibular afferents (Sadeghi et al. 2007) to potentially improve detection of weak signals. However, detailed calculations suggest that the total noise reduction may still not be sufficient for detection of distant prey (Ludtke and Nelson 2006; Maler 2009). Ludtke and Nelson (2006) have suggested, on theoretical grounds, that the P-unit spike patterning due to ISI correlations might provide the conditional probabilities that permit a small P-unit population to rapidly ($<$200 ms) detect very weak prey signals. These authors further suggested that a dynamic detection mechanism dependent on STD with ultra-rapid recovery was required for such detection; the hypothesized time scale of recovery was very similar to that demonstrated in this paper. Future work will be required to determine whether natural P-unit spike trains combined with FSTD and postsynaptic dynamics (NMDA receptors and voltage-gated ion channels) can implement a fast, low noise and ultra-sensitive detector that operates by computing the conditional probabilities of afferent spike trains.

P-units also encode the high-frequency EOD modulations associated with communication signals. In this case, their ISIs can transition from long ($>$10 ms) to very short ($<$4 ms) and back to long ($>$10 ms) again (Benda et al. 2006). Further work will be required to evaluate the effects of the FSTD on the encoding of high-frequency and transient electrosensory communication signals.

Our results have wider implications as well. It has long been thought that the dynamics of a neuron's spiking response (frequency-intensity or activation curve) were matched to the statistics of their sensory input (Bell and Sejnowski 1995; Chacron et al. 2005; Laughlin 1981; Srinivasan et al. 1982; Wark et al. 2009). We propose that this idea can be extended and that the temporal patterning of a neuron's spiking response is also matched to the dynamics of its synaptic output to target neurons.

ACKNOWLEDGMENTS

We thank M. Chacron for a careful reading of this manuscript and W. Ellis for general lab support.

GRANTS

This research was supported by a grant from Canadian Institute of Health Research to L. Maler and A. Longtin.

DISCLOSURES

No conflicts of interest are declared by the authors.

REFERENCES

Abbott LF, Regehr WG. Synaptic computation. *Nature* 431: 796–803, 2004.
Abbott LF, Varela JA, Sen K, Nelson SB. Synaptic depression and cortical gain control. *Science* 275: 220–224, 1997.
Akaike N, Hattori K, Oomura Y, Carpenter DO. Bicuculline and picrotoxin block gamma-aminobutyric acid-gated Cl- conductance by different mechanisms. *Experientia* 41: 70–71, 1985.
Bell AJ, Sejnowski TJ. An information-maximization approach to blind separation and blind deconvolution. *Neural Comput* 7: 1129–1159, 1995.
Bell CC, Maler L. *Central Neuroanatomy of Electrosensory Systems in Fish.* New York: Springer, 2005.

Benda J, Longtin A, Maler L. A synchronization-desynchronization code for natural communication signals. *Neuron* 52: 347–358, 2006.

Berman N, Dunn RJ, Maler L. Function of NMDA receptors and persistent sodium channels in a feedback pathway of the electrosensory system. *J Neurophysiol* 86: 1612–1621, 2001.

Berman NJ, Maler L. Inhibition evoked from primary afferents in the electrosensory lateral line lobe of the weakly electric fish (*Apteronotus leptorhynchus*). *J Neurophysiol* 80: 3173–3196, 1998a.

Berman NJ, Maler L. Interaction of $GABA_B$-mediated inhibition with voltage-gated currents of pyramidal cells: computational mechanism of a sensory searchlight. *J Neurophysiol* 80: 3197–3213, 1998b.

Berman NJ, Maler L. Distal versus proximal inhibitory shaping of feedback excitation in the electrosensory lateral line lobe: implications for sensory filtering. *J Neurophysiol* 80: 3214–3232, 1998c.

Berman NJ, Plant J, Turner RW, Maler L. Excitatory amino acid receptors at a feedback pathway in the electrosensory system: implications for the searchlight hypothesis. *J Neurophysiol* 78: 1869–1881, 1997.

Carlson BA. Temporal-pattern recognition by single neurons in a sensory pathway devoted to social communication behavior. *J Neurosci* 29: 9417–9428, 2009.

Chacron MJ, Longtin A, Maler L. Negative interspike interval correlations increase the neuronal capacity for encoding time-dependent stimuli. *J Neurosci* 21: 5328–5343, 2001.

Chacron MJ, Longtin A, Maler L. To burst or not to burst? *J Comput Neurosci* 17: 127–136, 2004.

Chacron MJ, Maler L, Bastian J. Electroreceptor neuron dynamics shape information transmission. *Nat Neurosci* 8: 673–678, 2005.

Chung S, Ferster D. Strength and orientation tuning of the thalamic input to simple cells revealed by electrically evoked cortical suppression. *Neuron* 20: 1177–1189, 1998.

Cook T, Pichaud F, Sonneville R, Papatsenko D, Desplan C. Distinction between color photoreceptor cell fates is controlled by Prospero in *Drosophila. Dev Cell* 4: 853–864, 2003.

Cupello A, Palm A, Rapallino MV, Hyden H. Can Cl- ions be extruded from a gamma-aminobutyric (GABA)-acceptive nerve cell via GABAA receptors on the plasma membrane cytoplasmic side? *Cell Mol Neurobiol* 11: 333–346, 1991.

Dittman JS, Regehr WG. Calcium dependence and recovery kinetics of presynaptic depression at the climbing fiber to Purkinje cell synapse. *J Neurosci* 18: 6147–6162, 1998.

Dobrunz LE, Huang EP, Stevens CF. Very short-term plasticity in hippocampal synapses. *Proc Natl Acad Sci USA* 94: 14843–14847, 1997.

Forsythe ID, Tsujimoto T, Barnes-Davies M, Cuttle MF, Takahashi T. Inactivation of presynaptic calcium current contributes to synaptic depression at a fast central synapse. *Neuron* 20: 797–807, 1998.

Fortune ES, Rose GJ. Short-term synaptic plasticity contributes to the temporal filtering of electrosensory information. *J Neurosci* 20: 7122–7130, 2000.

Gabbiani F, Koch C. Principles of spike train analysis. In: *Methods in Neuronal Modeling* edited by Koch C, Segev, I. Cambridge, MA: MIT Press, 1998. p. 313–360.

Goldman MS, Maldonado P, Abbott LF. Redundancy reduction and sustained firing with stochastic depressing synapses. *J Neurosci* 22: 584–591, 2002.

Gussin D, Benda J, Maler L. Limits of linear rate coding of dynamic stimuli by electroreceptor afferents. *J Neurophysiol* 97: 2917–2929, 2007.

Hermann J, Pecka M, von Gersdorff H, Grothe B, Klug A. Synaptic transmission at the calyx of Held under in vivo like activity levels. *J Neurophysiol* 98: 807–820, 2007.

Hjelmstad GO, Nicoll RA, Malenka RC. Synaptic refractory period provides a measure of probability of release in the hippocampus. *Neuron* 19: 1309–1318, 1997.

Hsu SF, Augustine GJ, Jackson MB. Adaptation of Ca(2+)-triggered exocytosis in presynaptic terminals. *Neuron* 17: 501–512, 1996.

Inomata N, Tokutomi N, Oyama Y, Akaike N. Intracellular picrotoxin blocks pentobarbital-gated Cl- conductance. *Neurosci Res* 6: 72–75, 1988.

Isaacson JS, Walmsley B. Amplitude and time course of spontaneous and evoked excitatory postsynaptic currents in bushy cells of the anteroventral cochlear nucleus. *J Neurophysiol* 76: 1566–1571, 1996.

Khanbabaie R, Mahani AS, Wessel R. Contextual interaction of GABAergic circuitry with dynamic synapses. *J Neurophysiol* 97: 2802–2811, 2007.

Krahe R, Bastian J, Chacron MJ. Temporal processing across multiple topographic maps in the electrosensory system. *J Neurophysiol* 100: 852–867, 2008.

Laughlin S. A simple coding procedure enhances a neuron's information capacity. *Z Naturforsch C* 36: 910–912, 1981.

Ludtke N, Nelson ME. Short-term synaptic plasticity can enhance weak signal detectability in nonrenewal spike trains. *Neural Comput* 18: 2879–2916, 2006.

Maler L. Receptive field organization across multiple electrosensory maps. II. Computational analysis of the effects of receptive field size on prey localization. *J Comp Neurol* 516: 394–422, 2009.

Marsat G, Proville RD, Maler L. Transient signals trigger synchronous bursts in an identified population of neurons. *J Neurophysiol* 102: 714–723, 2009.

Matveev V, Wang XJ. Implications of all-or-none synaptic transmission and short-term depression beyond vesicle depletion: a computational study. *J Neurosci* 20: 1575–1588, 2000.

Moortgat KT, Keller CH, Bullock TH, Sejnowski TJ. Submicrosecond pacemaker precision is behaviorally modulated: the gymnotiform electromotor pathway. *Proc Natl Acad Sci USA* 95: 4684–4689, 1998.

Nelson ME, MacIver MA. Prey capture in the weakly electric fish *Apteronotus albifrons*: sensory acquisition strategies and electrosensory consequences. *J Exp Biol* 202: 1195–1203, 1999.

Nelson ME, Xu Z, Payne JR. Characterization and modeling of P-type electrosensory afferent responses to amplitude modulations in a wave-type electric fish. *J Comp Physiol [A]* 181: 532–544, 1997.

Oleskevich S, Clements J, Walmsley B. Release probability modulates short-term plasticity at a rat giant terminal. *J Physiol* 524: 513–523, 2000.

Paolini AG, FitzGerald JV, Burkitt AN, Clark GM. Temporal processing from the auditory nerve to the medial nucleus of the trapezoid body in the rat. *Hear Res* 159: 101–116, 2001.

Ratnam R, Nelson ME. Nonrenewal statistics of electrosensory afferent spike trains: implications for the detection of weak sensory signals. *J Neurosci* 20: 6672–6683, 2000.

Rose GJ, Fortune ES. Frequency-dependent PSP depression contributes to low-pass temporal filtering in Eigenmannia. *J Neurosci* 19: 7629–7639, 1999.

Sadeghi SG, Chacron MJ, Taylor MC, Cullen KE. Neural variability, detection thresholds, and information transmission in the vestibular system. *J Neurosci* 27: 771–781, 2007.

Senn W, Segev I, Tsodyks M. Reading neuronal synchrony with depressing synapses. *Neural Comput* 10: 815–819, 1998.

Shadlen MN, Newsome WT. The variable discharge of cortical neurons: implications for connectivity, computation, and information coding. *J Neurosci* 18: 3870–3896, 1998.

Srinivasan MV, Laughlin SB, Dubs A. Predictive coding: a fresh view of inhibition in the retina. *Proc R Soc Lond B Biol Sci* 216: 427–459, 1982.

Stevens CF, Wang Y. Facilitation and depression at single central synapses. *Neuron* 14: 795–802, 1995.

Stevens CF, Wesseling JF. Activity-dependent modulation of the rate at which synaptic vesicles become available to undergo exocytosis. *Neuron* 21: 415–424, 1998.

Thomson AM, Deuchars J. Synaptic interactions in neocortical local circuits: dual intracellular recordings in vitro. *Cereb Cortex* 7: 510–522, 1997.

Tsodyks MV, Markram H. The neural code between neocortical pyramidal neurons depends on neurotransmitter release probability. *Proc Natl Acad Sci USA* 94: 719–723, 1997.

Wang Y, Manis PB. Short-term synaptic depression and recovery at the mature mammalian endbulb of Held synapse in mice. *J Neurophysiol* 100: 1255–1264, 2008.

Wark B, Fairhall A, Rieke F. Timescales of inference in visual adaptation. *Neuron* 61: 750–761, 2009.

Xu J, Wu LG. The decrease in the presynaptic calcium current is a major cause of short-term depression at a calyx-type synapse. *Neuron* 46: 633–645, 2005.

Yang H, Xu-Friedman MA. Relative roles of different mechanisms of depression at the mouse endbulb of Held. *J Neurophysiol* 99: 2510–2521, 2008.

Zucker RS, Regehr WG. Short-term synaptic plasticity. *Annu Rev Physiol* 64: 355–405, 2002.